Search for the elements 119 and 120

J. Khuyagbaatar,[1,2,*] A. Yakushev,[2] Ch.E. Düllmann,[1,2,3] D. Ackermann,[2,†] L.-L. Andersson,[1] M. Asai,[4] M. Block,[2] R.A. Boll,[5] H. Brand,[2] D.M. Cox,[6,‡] M. Dasgupta,[7] X. Derkx,[1,3] A. Di Nitto,[3,§] K. Eberhardt,[1,3] J. Even,[1,¶] M. Evers,[7] C. Fahlander,[8] U. Forsberg,[8] J.M. Gates,[9] N. Gharibyan,[10] P. Golubev,[8] K.E. Gregorich,[9] J.H. Hamilton,[11] W. Hartmann,[2] R.-D. Herzberg,[6] F.P. Heßberger,[1,2] D.J. Hinde,[7] J. Hoffmann,[2] R. Hollinger,[2] A. Hübner,[2] E. Jäger,[2] B. Kindler,[2] J.V. Kratz,[3] J. Krier,[2] N. Kurz,[2] M. Laatiaoui,[2] S. Lahiri,[12] R. Lang,[2] B. Lommel,[2] M. Maiti,[12,**] K. Miernik,[5] S. Minami,[2] A.K. Mistry,[2,6] C. Mokry,[1,3] H. Nitsche,[9,††] J.P. Omtvedt,[13] G.K. Pang,[9] P. Papadakis,[6,14] D. Renisch,[3] J. Roberto,[5] D. Rudolph,[8] J. Runke,[2] K.P. Rykaczewski,[5] L.G. Sarmiento,[8] M. Schädel,[2,4] B. Schausten,[2] A. Semchenkov,[13] D.A. Shaughnessy,[10] P. Steinegger,[15,16] J. Steiner,[2] E.E. Tereshatov,[10,‡‡] P. Thörle-Pospiech,[1,3] K. Tinschert,[2] T. Torres De Heidenreich,[2] N. Trautmann,[3] A. Türler,[17,16] J. Uusitalo,[14] M. Wegrzecki,[18] N. Wiehl,[1,3] S.M. Van Cleve,[5] and V. Yakusheva[1]

[1] *Helmholtz Institute Mainz, 55099 Mainz, Germany*
[2] *GSI Helmholtzzentrum für Schwerionenforschung, 64291 Darmstadt, Germany*
[3] *Johannes Gutenberg-Universität Mainz, 55099 Mainz, Germany*
[4] *Advanced Science Research Center, Japan Atomic Energy Agency, Tokai, Ibaraki 319-1195, Japan*
[5] *Oak Ridge National Laboratory, Oak Ridge, TN 37831, USA*
[6] *University of Liverpool, Liverpool L69 7ZE, United Kingdom*
[7] *Department Nuclear Physics, RSP, The Australian National University, Canberra, ACT 2601, Australia*
[8] *Lund University, 22100 Lund, Sweden*
[9] *Lawrence Berkeley National Laboratory, Berkeley, CA 94720, USA*
[10] *Lawrence Livermore National Laboratory, Livermore, California 94551, USA*
[11] *Vanderbilt University, Nashville, TN 37235, USA*
[12] *Saha Institute of Nuclear Physics, Kolkata 700064, India*
[13] *University of Oslo, 0315 Oslo, Norway*
[14] *University of Jyväskylä, 40351 Jyväskylä, Finland*
[15] *Paul Scherrer Institute, 5232 Villigen PSI, Switzerland*
[16] *University of Bern, 3012 Bern, Switzerland*
[17] *Paul Scherrer Institute, 5232 Villigen, Switzerland*
[18] *Łukasiewicz - Institute of Electron Technology, 02-668 Warsaw, Poland*

(Dated: September 10, 2020)

A search for production of the superheavy elements with atomic numbers 119 and 120 was performed in the ^{50}Ti+^{249}Bk and ^{50}Ti+^{249}Cf fusion-evaporation reactions, respectively, at the gas-filled recoil separator TASCA at GSI Darmstadt, Germany. Over four months of irradiation, the ^{249}Bk target partially decayed into ^{249}Cf, which allowed for a simultaneous search for both elements. Neither was detected at cross-section sensitivity levels of 65 and 200 fb for the ^{50}Ti+^{249}Bk and ^{50}Ti+^{249}Cf reactions, respectively, at a mid-target beam energy of $E_{\rm lab}$ = 281.5 MeV. The non-observation of elements 119 and 120 is discussed within the concept of fusion-evaporation reactions including various theoretical predictions on the fission-barrier heights of superheavy nuclei in the region of the island of stability.

PACS numbers: Valid PACS appear here

I. INTRODUCTION

To date, 118 chemical elements are known. They fill the periodic table of the elements until the end of the seventh row. The heaviest elements with proton numbers $Z = 114 - 118$ have been synthesized only in fusion reactions of the doubly magic ^{48}Ca ($Z = 20$) nucleus with nuclei of radioactive isotopes of actinide elements from plutonium ($Z = 94$) to californium ($Z = 98$) [1, 2]. Elucidating the nuclear, atomic, and chemical properties of superheavy elements (SHEs) are fundamental quests in chemistry and physics [2–4]. One of the main goals of SHE research is the search for an island of stability arising from the presence of closed nuclear shells, which are predicted to inhibit spontaneous fission of the superheavy

* J.Khuyagbaatar@gsi.de
† Present address:GANIL, CEA/DSM-CNRS/IN2P3, Bd Henri Becquerel, BP 55027, F-14076 Caen Cedex 5, France
‡ Present address:Lund University, 22100 Lund, Sweden
§ Present address:Universitá degli Studi di Napoli "Federico II", 80126 Naples, Italy
¶ Present address:University of Groningen, 9747 AA Groningen, The Netherlands
** Present address: Indian Institute of Technology Roorkee, Roorkee 247667, India.
†† deceased
‡‡ Present address:Cyclotron Institute, Texas A&M University, College Station, TX, 77843, USA

nuclei (SHN).

Currently available experimental data on the decay properties of known superheavy nuclei [1, 5–16] indicate a stability against fission, thus confirming the concept of the island of stability. But to date, the exact location of the center of the island of stability, i.e., proton and neutron shell closures, and its landscape are not yet known. For a long time it was assumed that $Z = 114$ and neutron number $N = 184$ would form closed shells [3]. However, current information from experimental data and modern theoretical calculations do not exclude that the next closed proton shell occurs at $Z > 118$ [4]. From chemical and atomic perspectives, SHEs beyond oganesson (Og, $Z = 118$) will start the eighth row in the periodic table. Data on SHE from the eighth row are of great interest for the verification of the periodicity of the elements and the influence of relativistic effects on chemical properties [2].

The synthesis of SHEs beyond Og faces, however, many experimental challenges. One of them is the need to use fusion-evaporation reactions with projectiles heavier than ^{48}Ca [17–19], because of insufficient amounts of materials of elements with appropriate proton numbers, $Z > 98$, to make a target [20]. With this constraint, the four different reactions ^{64}Ni+^{238}U [21], ^{58}Fe+^{244}Pu [22], ^{54}Cr+^{248}Cm [23], and ^{50}Ti+^{249}Cf [24] have already been examined for the synthesis of SHE with $Z = 120$. However, none of these experiments provide evidence for the synthesis of the new element.

The use of ^{50}Ti as a projectile and ^{249}Bk and ^{249}Cf as targets appear to be the most promising combinations for the synthesis of elements 119 and 120 [17–19, 25]. ^{249}Bk, which decays by β^- into ^{249}Cf with a half-life of only 327.2(3) d [26] is a unique target. Starting with a freshly prepared, pure ^{249}Bk target, the amount of ^{249}Bk will continuously decrease over time, and the amount of ^{249}Cf will increase [16]. This situation provides a unique opportunity to simultaneously search for a direct production of two SHEs in a single long-lasting irradiation. This was the case in the bombardment of a ^{249}Bk target by ^{48}Ca, where the two elements tennessine (Ts, $Z = 117$) and Og were observed as evaporation residues (ERs) from the ^{48}Ca+^{249}Bk and ^{48}Ca+^{249}Cf reactions, respectively [27].

By exploiting this feature of the ^{249}Bk target material, we searched for the SHEs with $Z = 119$ and 120 in a four-months long experiment with a ^{50}Ti beam.

II. EXPERIMENTAL SETUP AND CONDITIONS

Isotopically pure ^{249}Bk target material was produced at Oak Ridge National Laboratory (ORNL), USA [20] and a sample of 12 mg was shipped to Johannes Gutenberg-Universität Mainz, Germany, for the target production. Four banana-shaped target segments with thicknesses of 0.37(4), 0.53(5), 0.53(5), 0.50(5) mg/cm^2 were produced by molecular plating [28] on 0.99(5) mg/cm^2 Ti-backing foils, each with an area of 6 cm^2. The average areal density of the target was 0.48(5) mg/cm^2. Because of the relatively short half-life of ^{249}Bk, it was essential to start the experiment as soon as possible to maximize the probability for the discovery of element 119. Target irradiation started within about one month after the target production [29].

The evolution of the areal densities of ^{249}Bk and ^{249}Cf in the target is shown in Fig. 1(a). One can see that the target with an average areal density of 0.48(5) mg/cm^2 consisted of $\approx$ 0.43 mg/cm^2 ^{249}Bk at the beginning of the experiment. This converted slowly into ^{249}Cf. At the end of the experiment the ingrowth of ^{249}Cf reached $\approx$ 0.17 mg/cm^2. The four target segments were mounted on a wheel, which rotates synchronously to the time structure of the beam. To ensure safe operation, all target segments were continuously monitored using different methods such as online temperature readings during the experiment with a pyrometer [16, 30].

Prior to the experiment, a high-intensity and long-term stable ^{50}Ti beam was developed and established at GSI. A heavy-ion beam of ^{50}Ti with charge state 2^+ was produced in a Penning ion-source. These ions, further, were stripped to a charge state 12^+ and accelerated by the UNIversal LInear ACcelerator (UNILAC) in a pulsed mode with 5 ms pulse length and 50 Hz repetition frequency to an energy of 300 MeV. A total beam dose of 3.6×10^{19} particles passing the target was accumulated in two experimental campaigns, which overall resulted in about four months of irradiation. The average intensity of beam on target was about 0.65 particle μA (4×10^{12} particles/s). In Fig.1(b), the chronology of beam intensity over the whole four-months period is shown. To maintain a high-beam intensity over a long time period, fresh ion-source material was supplied daily.

Before impinging on the target, the beam passed through a 50-μg/cm^2 thin carbon foil mounted on a wheel on the same axis as the target wheel, with both wheels rotating synchronously. The carbon foil was used as a charge stripper for ^{50}Ti^{12+} ions to ensure their safe deflection in the dipole magnet into the direction of the beam stop. The beam energy in the center of the target was estimated by using the SRIM code [31]. Energy losses of the initial beam in the carbon and titanium foils were directly calculated using the database of SRIM. For calculation of the energy loss in the actinide target, its most probable chemical composition in forms of $^{249}Bk_2{}^{16}O_3$ and $^{249}Cf_2{}^{16}O_3$ was used, and the proper ratio of ^{249}Bk to ^{249}Cf atoms in the target was taken into account. The average beam energy was calculated at $E_{\rm lab}$ = 281.5 MeV in the center of the target (laboratory frame), which is not affected by variation of the fractions of ^{249}Bk and ^{249}Cf in the target. Beam energies entering and leaving the target are 283.9 and 279.1 MeV, respectively.

The excitation energies of the compound nuclei (CN) $^{299}119^*$ and $^{299}120^*$, which could be produced in the

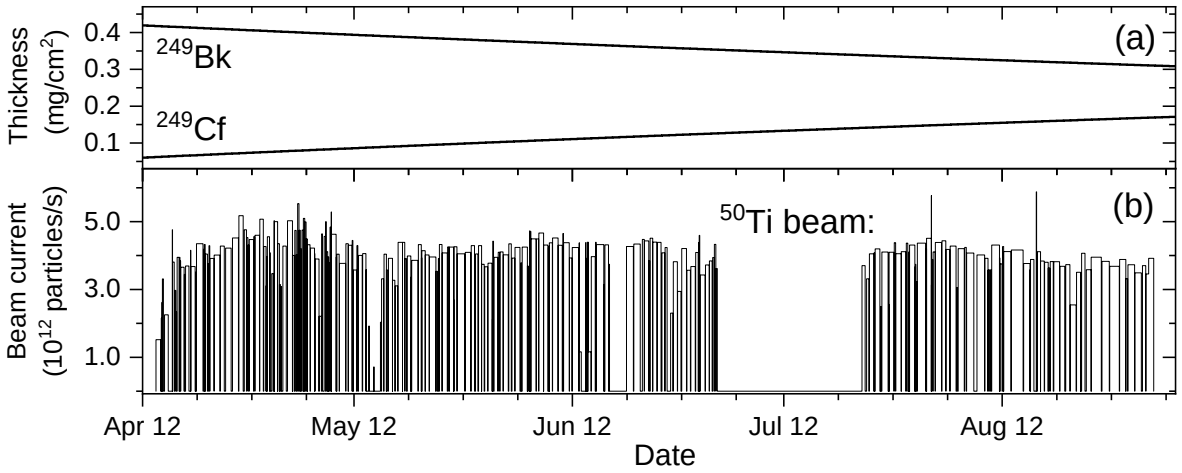

FIG. 1. (a) Chronological evolutions of isotopic thicknesses of ^{249}Bk and ^{249}Cf with an average total thickness of 0.48(5) mg/cm^2 during the irradiations with the ^{50}Ti beam with an energy of E_{lab} = 281.5 MeV in the middle of the target. (b) ^{50}Ti beam current on target averaged over time of each set of the irradiation.

fusion of ^{50}Ti with ^{249}Bk and ^{249}Cf, respectively, were estimated by using the known experimental mass excesses of projectile and target nuclei [32] and theoretical values from Ref. [33] for the CN. With the mid-target beam energy of E_{lab} = 281.5 MeV, excitation energies of E^* = 43.2 MeV and 37.6 MeV result for $^{299}119^*$ and $^{299}120^*$, respectively. At these excitation energies the 3n and/or 4n evaporation channels are expected to be predominant and corresponding heavy ERs should be observed [1, 34].

The gas-filled recoil separator TASCA [12, 35] was filled with helium gas at 0.8 mbar pressure. Its magnetic fields were set to guide heavy ions with a magnetic rigidity of $B\rho$ = 2.16 Tm [36] to the center of the focal plane detector. This magnetic rigidity ensures a safe isolation of ERs from both fusion reactions from the primary beam and products of other reaction channels like elastic and (deep) inelastic scattering [37, 38]. The efficiency of TASCA for the collection of ERs from the ^{50}Ti+^{249}Bk/^{249}Cf reactions was estimated by performing Monte-Carlo simulations [37]. An average transmission of 55% was derived for the applied experimental conditions and taking into account theoretical predictions on the shape of the ER excitation functions for the ^{50}Ti+^{249}Bk/^{249}Cf reactions [34].

The ERs passing through TASCA entered the detector chamber and first passed through a multi-wire proportional counter (MWPC). The anode signal was read out and stored in coincidence within about 5 μs to any event registered in the implantation detector.

The focal plane detection system (FPDS) of TASCA consisted of a double-sided silicon strip detector (DSSD)-based implantation detector (hereafter: stop detector), with eight DSSDs (hereafter: box detectors) mounted perpendicular in the backward hemisphere of the stop detector to form a five-sided box configuration. The stop detector comprised 144 vertical (X) and 48 horizontal (Y) 1-mm strips on the front and back sides, respectively. The 144 vertical strips faced TASCA and have 0.1 mm inter strip pitch. The 48 horizontal strips provide the position information along the Y-axis. Each box detector was 72×48 mm^2 in size and had 16 strips on each side, oriented perpendicular to each other. The longer strips were faced inside the box configuration. In the data processing, signals from every two neighboring strips of the box detectors were combined. Detailed descriptions of the FPDS are given in Refs. [39, 40]

Two adjacent single-sided Si-strip detectors having together the same size as the stop detector were mounted directly behind the stop detector to register particles passing through the stop detector (veto detector). The veto detector was used to discriminate real α events from low energy signals originating from light charged particles passing through the separator and the stop detector [9].

The Combined ANalog and DIgital (CANDI) [41] data acquisition system was used for processing the data collected with the FPDS. Signals from the front 144 vertical strips of the DSSD, box, veto, and MWPC detectors were processed in a standard way, i.e., pre-amplified, amplified and shaped, and digitized by using peak-sensing ADCs. All pre-amplified signals were duplicated. Spectroscopic amplifiers with two gains differing by a factor eleven were used to create two branches for energies of α particles and for high-energetic particles, respectively. These signals were independently stored in the analog part of the CANDI, which had a dead-time of $\approx$ 35 μs. Pre-amplified signals from the horizontal strips of the stop detector were digitized by 60 MHz-sampling ADCs by storing their shapes in 50 μs-long traces (8 μs before and 42 μs after the trigger). Finally, data streams from analog and digital DAQs connected to the FPDS were combined as single data, which allowed the determination of the time, spatial coordinates, beam-on/off status, energy, and shape of each detected event [42]. The advantages of CANDI-type systems for the solution of various

physics and measurement technical issues and for superheavy element search experiments are demonstrated in Refs. [11–13, 16, 41, 43–46].

The efficiency for the detection of α particles with full energy emitted by nuclei implanted in the FPDS is estimated to be 76(4)%. The efficiency for the detection of fission events is 100%. The energy resolution (FWHM) of individual strips of stop and box detectors prior to the experiment was $\approx$ 40 keV for 5.8 MeV α particles from an external α source placed in front of the DSSD. The final energy calibrations were done using the α decays of nuclei produced in a preparatory irradiation using the ^{50}Ti+^{176}Yb reaction [41]. In case of the Y-strips of the DSSD, the full energy of an event was sometimes shared between two neighboring strips while the energy from the front side was collected by a single X-strip. On average, such split signals were observed in 16% of all cases throughout all Y-strips. The data acquisition was triggered by any event registering more than about 600 keV in a front (X) and/or more than about 500 keV in a back (Y) strip of the stop detector.

Calibration of the high-energy branch was done with an external four α-line source [5]. With such a calibration, the measured energies of fission fragments from ^{256}Rf were distributed in the range of 50-200 MeV [44].

III. EXPERIMENTAL RESULTS: SEARCH FOR ELEMENTS 119/120 IN THE CORRELATION ANALYSES

The low-energy spectrum (analog part of the data stream) of events registered during the 15 ms beam-off period after each 5 ms pulse is shown in Fig. 2. This spectrum clearly shows the peaks and pileup events corresponding to α decays of non-fusion products originating from both ^{50}Ti+^{249}Bk/^{249}Cf reactions. A detailed investigation of such non-fusion products from the ^{50}Ti+^{249}Cf reaction obtained at TASCA was carried out in Ref. [43]. The nuclei produced in the present experiment as products of non-fusion reactions were similar to this ^{50}Ti+^{249}Cf study [43].

Usually, beam-off events are the main source (up to $\approx$ 75%) s for finding genetically correlated α particles originating from the decays of implanted nuclei with half-lives longer than $\approx$ 5 ms. The remaining $\approx$ 25% of α decays occur during the 5 ms beam-on periods. Events detected during beam-on periods without a coincident MWPC signal are also shown in Fig. 2. They were also taken into account in the correlation analysis.

In general, the analysis procedure to search for α-decay chains was the same as the one described in Ref. [16], except for the selected energy windows for the α-like events. It is noteworthy that the identification of α-decay chains originating from SHN with $Z = 119$ is supposedly relatively simple, since these SHN and their Ts daughters are expected to undergo α decay with half-lives less than 1 s [47] and decay properties of their progenies ^{287,288}Mc

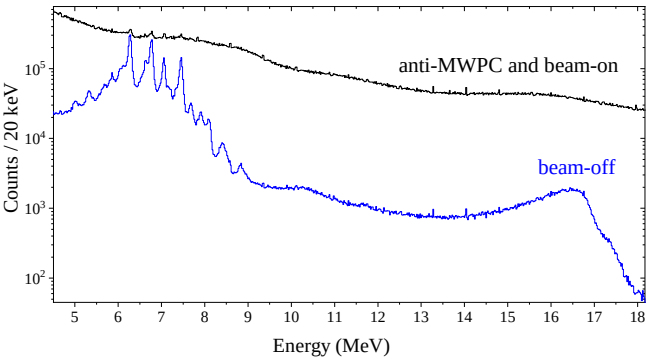

FIG. 2. (color online) Low-energy spectra of all beam-off and anti-MWPC beam-on events measured during the entire four-months run.

are known [1]. In the case of the $Z = 120$ nuclei, we do not exclude to observe α-decay chains starting only from the hitherto unknown daughters ^{291,292}Og ($Z = 118$), because the half-lives of the $Z = 120$ mothers could be very short [47, 48]. This might lead to decay before the implantation in the stop detector has occurred. However, if these short-living $Z = 120$ nuclei can survive $\approx$0.6 μs flight time through TASCA, then the CANDI system would allow their decay to be resolved down to time differences of about 100 ns between the implantation and decay as was demonstrated for short-lived nuclei near the closed $N = 126$ shell region [41]. If the half-lives of $Z = 120$ nuclei were less than $\approx$0.6 μs then the calculated 55% TASCA transmission would be reduced by a factor more than two.

By taking into account various possible scenarios for the expected decay chains, we performed various position- and time-correlation analyses between implantation (ER), α, and fission-like (SF) events to find chains of non-random origin. Correlation analyses searching for ER–α_1–α_2 ($\Delta t_{ER-\alpha_1} < 1$ s, $\Delta t_{\alpha_1-\alpha_2} < 20$ s) and ER–α_1–α_2–SF ($\Delta t_{ER-\alpha_1} < 20$ s, $\Delta t_{\alpha_1-\alpha_2} < 300$ s, $\Delta t_{\alpha_2-SF} < 500$ s) were used. The energy conditions for the first and second α-like events were 8.5-13.0 MeV. As the energy ranges are the same and the searching times are long, the random correlation rate was relatively high, especially for α-like events detected during beam-on periods. However, these search conditions ensure that also all non-random decay chains with 'missing' member(s), e.g., α particles escaping into the backward open hemisphere of the FPDS, will be found.

Any event with energies 3-20 MeV and coincident to an MWPC signal was considered to be an ER-like event [16]. Average counting rates of ER-like, α-like, and SF events per pixel of the stop detector during the beam-on and beam-off periods were similar to that for the ^{48}Ca+^{249}Bk reaction (see [16]).

Only randomly correlated events similar to the ones found in the ^{48}Ca+^{249}Bk reaction measured at TASCA were observed. A detailed discussion on the origin of random events is given in Ref. [16]. Finally, as a result

of these analyses, no correlated ER, α, and SF events, having decay properties of SHN and originating from the expected α-decay chains of ^{295,296}119 and ^{295,296}120, were detected [1, 16]. We determined a cross section value for the observation of one event (hereafter: cross-section sensitivity) by taking into account the variations of the ^{249}Bk and ^{249}Cf target thicknesses over time as shown in Fig. 1, and the efficiencies of TASCA and the FPDS given in Sec. 2. For the ^{50}Ti+^{249}Bk reaction the cross-section sensitivity reached 65 fb, and for the ^{50}Ti+^{249}Cf reaction it was 200 fb.

It is worth noting that these cross-section sensitivity levels are applicable only in the cases, where the isotopes of elements 119 and 120 decay by α-particle emission. In the case of their fission decay for which recent calculations show non-negligible probabilities [49, 50], the present experiment was not sensitive enough to identify an origin of fission events in the ER–SF correlation analysis. This was due to a large number of fission events (in total twenty-five thousands) originating from the decay of target-like nuclei produced in transfer reactions [16].

IV. DISCUSSION

In the present experiment relatively low cross-section sensitivities were reached, however elements 119 and 120 were not detected. The reached cross-section sensitivities together with the ones reached for three other reactions leading to element 120 [21–23] reveal the impact of the change of the projectile and of the compound nucleus' Z in the fusion-evaporation reaction. Practically, it means a deviation of cross sections for reactions with heavier projectiles from the well known ^{48}Ca-induced reactions. Accordingly, the results shall be discussed relative to the known properties of the ^{48}Ca-induced reactions. Such a comparative analysis was made in Refs. [18, 19]. The maximum cross sections of fusion-evaporation reactions with certain projectile or target nuclei exhibit well pronounced trends as a function of the Coulomb parameter, $Z_pZ_t/(A_p^{1/3} + A_t^{1/3})$. In Fig. 3(a), all known maxima of either σ_{3n}(max) or σ_{4n}(max) from the ^{48}Ca-induced reactions [1, 5–16, 51] leading to the formation of SHN are shown as a function of the Coulomb parameter. Only cross-section sensitivities are known for the ^{48}Ca+^{232}Th reaction [52]. In addition, the σ_{3n} value from the ^{48}Ca+^{197}Au reaction [53] is shown to explore a systematic trend in a wider range of the Coulomb parameter. The present cross-section sensitivities together with those of the other three reactions leading to element 120 [21–23] are also shown in Fig. 3(a). It is important to mention that despite the different projectile and target nuclei, all these reactions share one common feature: all target nuclei are deformed.

All features seen in Fig. 3(a) are due to properties of the fusion-evaporation reaction, which consists of three subsequent processes: capture, fusion and the compound nucleus' de-excitation. Accordingly, the ER cross section is described by the three-term expression

$$\sigma_{ER}(E^*) = \sum \sigma_{cap}(E_{c.m.}, J) P_{CN}(E_{c.m.}, J) W_{CN}(E^*, J), \quad (1)$$

where σ_{cap} is the cross section characterizing two captured nuclei forming a composite system at a collision energy $E_{c.m.}$, P_{CN} is the fraction of composite systems that forms a CN, and W_{CN} is the survival probability of the CN against fission through particle evaporation at excitation energy $E^* = E_{c.m.} - Q$ and angular momentum J. Q is the mass difference between the sum of reactant nuclei and the CN. In the case of the heaviest nuclei, mostly neutrons are evaporated [5, 54–56] leading to a preferential and almost exclusive population of neutron evaporation channels (xn channels). Thus, discussing ERs of the fusion reaction leading to SHE, we refer to all possible neutron-evaporation channels (xn-channels).

The terms σ_{cap} and W_{CN} describe independent processes and have been studied substantially, both experimentally and theoretically. Many theoretical calculations describe the known σ_{xn} values of the ^{48}Ca-induced reactions fairly well. However, their predictions for the elements 119 and 120 have large deviations of several orders of magnitude. Thus, the predictive power of those calculations is limited and needs to be verified experimentally. Thus, the choice of any particular theoretical result as a baseline for the planning of a new-element search experiment becomes somewhat arbitrary. A systematic analysis of accumulated experimental data on the fusion-evaporation reactions as given in Fig. 3(a) could be useful for the planning of the experiment, and also for the discussion of the obtained results.

As seen from Eq. 1, essential for the observation of the desired ER is a proper choice of the beam energy ($E_{c.m.}$ or E^*). Our results, i.e., the non-observation of ERs, do not allow any conclusion to be drawn about the proper choice of beam energy, which matched the maximum of a calculated 4n-evaporation excitation function of the ^{50}Ti+^{249}Bk reaction [34]. The maximum cross-section values shown in Fig. 3(a) correspond to various projectile energies, each optimal for a given reaction and CN. In fact, in almost every ^{48}Ca+actinide reaction, ERs were observed at projectile energies up to 10 MeV above the fusion barrier (V_B) [57], i.e., (1.00–1.07)$\cdot V_B$ [1, 58, 59]. These energies then correspond to E^* in the range of 35-45 MeV. This shows that E^* within this range does not drastically affect the final results of these fusion-evaporation reactions, i.e., the σ_{ER}. However, it does affect each term of Eq. 1. Projectile energies greater than V_B ensure large σ_{cap}, which drops drastically below the barrier and increases exponentially as a function of $E_{c.m.}$ [60]. The recently measured barrier distribution of the ^{48}Ca+^{248}Cm reaction shows that the distribution's centroid is located at an energy slightly greater than V_B [58]. This is due to the deformation of the target nucleus, which provides two distinct collision geometries:

tip and side. The side-collision, which is predicted to be the main source for fusion according to time dependent Hartree-Fock calculations [61], results in a larger potential barrier for the fusion than the tip-collision and V_B calculated for spherically shaped nuclei [57]. Thus, observation of ERs in ^{48}Ca+actinide reactions at energies of (1.00–1.07)·V_B is seemingly also due to an increase in P_{CN} as a function of $E_{c.m.}$ [62]. Finally, the survival probability of the CN is reduced with an increase of E^*. Thus overall, the three terms in Eq. 1 compensate each other as a function of $E_{c.m.}$, which leads to a broad energy range for observing ERs.

From a nuclear reaction point of view (σ_{cap} and P_{CN}), one can assume that the present ^{50}Ti+^{249}Bk and ^{50}Ti+^{249}Cf reactions are similar to the ^{48}Ca-induced reactions because of the target deformation. There should be some deviations due to the influence of the nuclear structure of the reactants, which largely impacts fusion-evaporation cross sections in Pb-target based reactions [60, 63–65] but is not yet fully understood in reactions with deformed target nuclei [66, 67]. Nevertheless, broad ER excitation functions of the present reactions, similar to the ones for ^{48}Ca-induced reactions can be assumed. Theory supports such a conclusion [34, 68–72]. The beam energy, which we chose for the ^{50}Ti+^{249}Bk and ^{50}Ti+^{249}Cf reactions corresponds to $\approx 1.05 \cdot V_B$ ($V_B = 223.7$ MeV) and $1.04 \cdot V_B$ ($V_B = 226.2$ MeV), respectively. These values are within the above mentioned energy range where fusion is predicted to be enhanced according to the results from the experiment [58] and the theory [61]. Therefore, it is unlikely that the used beam energy was the major reason for the non-observation of elements 119 and 120. More likely, it is due to the very low cross sections of these reactions, which have their origin in the fusion-reaction mechanism and the survival probability of the fused system.

The fusion probability of the two nuclei predominantly depends on the Coulomb force between the reactants. The composite system, which consists of many protons and neutrons often fails to form a CN under the influence of the resulting total Coulomb force and system reseparates. This so-called quasi-fission (QF) process has been known for decades and has been investigated in details [17, 25, 66, 76–79]. The presence of QF ($P_{CN} < 1$) had been predicted theoretically for reactions with a projectile-target charge product $Z_pZ_t \geq 1600$ [76]. To date, this limit has been altered and QF has been proven to also be present in reactions having much smaller Z_pZ_t values [63, 80–82]. All reactions given in Fig. 3(a) have Z_pZ_t values exceeding the original threshold value (except for the case of ^{197}Au). Thus, QF can be expected to be dominant over fusion as was also experimentally shown [17, 66, 78, 79, 83, 84]. In general, a quantitative estimate of the QF probability as a function of Z_pZ_t is a very complex problem and intensive research on this topic is still ongoing. In Refs. [34, 83], semi-empirical estimates are given that are based on the P_{CN} values deduced from the experimental data.

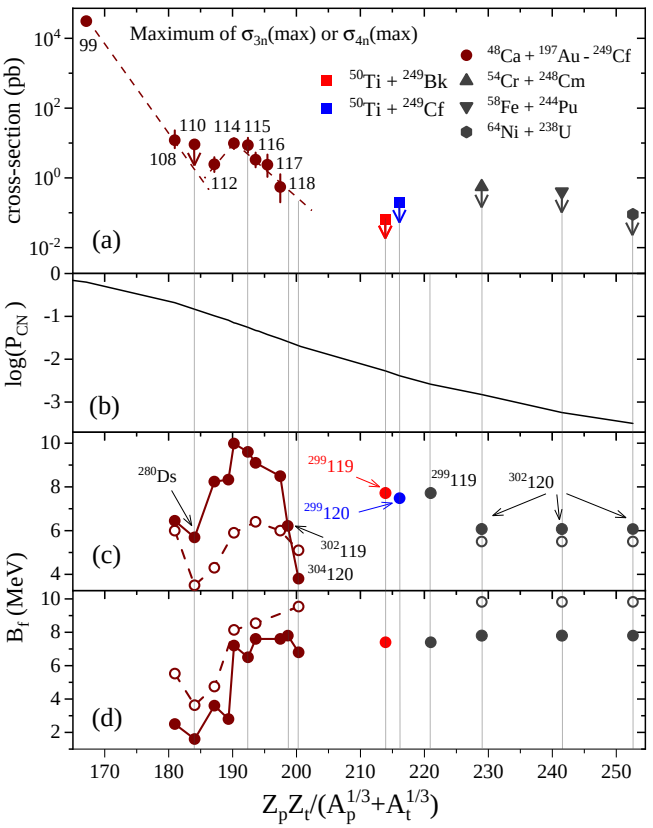

FIG. 3. (color online) (a) Compiled data showing the greater value of the either maximum σ_{3n} or maximum σ_{4n} of ^{48}Ca-induced reactions with actinide targets [1, 5–16, 51] and with ^{197}Au [53]. Present experimental cross-section sensitivities for ^{50}Ti+^{249}Bk and ^{50}Ti+^{249}Cf are shown together with those of the ^{54}Cr+^{248}Cm [23], ^{58}Fe+^{244}Pu [22], ^{64}Ni+^{238}U [21] and ^{48}Ca+^{232}Th [52] reactions. Proton numbers of observed ERs from these reactions are indicated. (b) Calculated P_{CN} values according to Ref. [34]. (c) Theoretical B_f values from two different macro-microscopic models. Solid and open symbols are the results from Refs. [73] and [48], respectively. Compound nuclei of reactions, which have not yet resulted in the detection of SHN are given, too. (d) Theoretical B_f values from two different microscopic models. Solid and open symbols are from Refs. [74] and [75], respectively. Vertical lines indicate the Coulomb parameters of the reactions leading to the compound nuclei marked in (c). See text for details.

By using the expression given in Ref. [34] to estimate the P_{CN} values for actinide-target based reactions, P_{CN} was calculated for all reactions shown in Fig. 3(a). The results are shown in Fig. 3(b). P_{CN} values are exponentially decreasing as a function of the Coulomb parameter. This is in agreement with the trend of the σ_{xn} values, which decreases exponentially ([18, 19]) until Hs [cf. Figs. 3(a) and 3(b)]. It also shows that a change of a few protons in the target's Z with a fixed projectile nucleus does not lead to a significant variation of the Coulomb parameter because of the large numbers of initial protons. For instance, a change from ^{232}Th (leading to formation of ^{280}Ds*) to ^{243}Am (^{291}Mc*) is a 4.7% change in the tar-

get's Z, which results in a decrease in P_{CN} by a factor of about three in the ^{48}Ca-induced reactions.

However, in the ^{48}Ca+^{232}Th reaction, for which fusion is more favorable, the element Ds was not observed at a cross-section sensitivity of about 9 pb [52], which is close to the maximum σ_{xn} value obtained for the ^{48}Ca+^{243}Am reaction [1, 13]. In fact, for the reactions leading to SHEs heavier than Ds the trend of an exponential decrease in σ_{xn} values is broken and the maximum cross section remains at a level of $\approx 0.5 - 10$ pb with a local maximum at $Z \approx 114$. This feature, i.e., a sudden increase in the ER cross sections relative to a decreasing trend, was discussed in connection with the survival probability of the CN [1, 18].

Once the compact-shaped CN is formed and at full equilibrium in all internal degrees of freedom as a result of fusion, it has an excitation energy that will be released via fission, emission of light particles, and/or electromagnetic transitions [57, 62]. Each reaction shown in Fig. 3 has been measured at CN excitation energies greater than 30 MeV, which significantly exceeds the height of the fission barrier, B_f, and the neutron and the proton separation energies of the CN. The survival probability of the superheavy CN is often expressed as

$$W_{CN}(E^*) \sim \prod_{i=1}^{x} e^{[(B_f - S_n)/T]_i},$$

where T and x are the temperature and the number of emitted neutrons, respectively. Here, one should note that the successive emission of neutrons at each i-th step forms a 'new' CN, which has to survive against multichance fission processes. Recently, the interest in multichance fission in the de-excitation of the CN has been renewed due to experimental evidence showing significant contributions of this process in fusion-fission [63] and transfer-induced fission [85, 86] reactions. However, the crucial point remains the survival probability of the initially formed CN, where both E^* and J are high [63, 85]. Accordingly, the B_f of the initial CN is one of the important quantities for the survival process [18, 63, 85].

To shed some light on the dependence of the σ_{xn} value (which reflects the survival probability of the excited CN) on the CN's fissility, we show in Figs. 3(c) and 3(d) calculated B_f values for the CN formed in each reaction shown in Fig. 3(a). We selected four different theoretical values for the fission barriers as representatives of two main theoretical approaches, i.e., macro-microscopic [48, 73] and microscopic [74, 75] ones. Presently, many other theoretical predictions performed within these two approaches exist (see [87–90] and references therein) and their results are equally valid as those selected in this work and will not affect on quality of the discussion.

All calculations predict an increase of B_f in nuclei of the elements above Ds. This indicates that their stability against fission is enhanced due to the shell effects related to the island of stability [1, 18]. Such an increase in the predicted B_f values can be the reason for a sudden increase in the measured ER cross sections, which are due to the enhanced survival probability. Moreover, the non-observation of Ds-nuclei in the ^{48}Ca+^{232}Th reaction at the cross section level of about 9 pb can be explained by their low B_f value, which is barely affected by the shell effects originating from the island of stability.

However, the results of different theoretical frameworks deviate in the prediction of the B_f values for SHN, and at which Z the next shell closure will occur. According to macro-microscopic models, the effect of the enhanced fission barrier is most dominant in Fl nuclei and decreases towards heavier SHN. A similar trend is observed in experimental σ_{xn} values as shown in Fig. 3(a). The self-consistent purely microscopic models predict the B_f values for the elements 119 and 120 to be similar to, or greater than those in the range of Fl to Og. Overall, the results obtained in both frameworks are able to explain the observed trend of the σ_{xn} values up to Og. Supposedly, an increase in B_f values of these SHN results in an increase of W_{CN}, which counteracts a reduction in P_{CN}. In this case, the above mentioned factor of about three in decrease in P_{CN} from ^{48}Ca+^{232}Th to ^{48}Ca+^{243}Am may be compensated by an increase in the B_f values in both models. However, not in all calculations B_f values significantly increase beyond Og. This leads to the assumption that the upper limit for the gain in W_{CN} for SHN with $Z = 119$ and 120 is the same as for the ^{48}Ca-induced reactions. However, the question is whether this gain can completely compensate a reduction in P_{CN} or not.

The present two reactions show a reduction in P_{CN} by a factor of more than five compared to any of the measured ^{48}Ca-induced reactions. Such a strong reduction is due to the relatively large change in the Coulomb parameter that originates from the ≈ 4.2 % change in the projectile's Z. One can estimate that the reduction in σ_{xn} is at least about a factor of ≈ 5.6, which is the relative decrease in P_{CN} for ^{50}Ti+^{249}Bk compared to the ^{48}Ca+^{249}Cf reaction, where the element Og was produced with $\sigma_{3n} \approx 0.5$ pb. This translates to the necessity to reach a cross-section sensitivity on the order of 90 fb. This value indeed has been reached in this experiment for element 119 (65 fb). However, the absence of any detected event indicates that σ_{xn} may decrease stronger than suggested by the P_{CN} estimation given in Ref. [83]. A rapid decrease in P_{CN} would favor the results of the microscopically calculated B_f shown in Fig. 3(d) for the synthesis of the elements beyond Og. At the same time, the macro-microscopic results for B_f do not exclude a further reduction of σ_{xn} for the syntheses of the elements 119 and 120 in each projectile-target combination in addition to the reduction due to the change in P_{CN}. Eventually, this raises interest in measuring cross sections of the ^{48}Ca+^{254}Es and ^{48}Ca+^{257}Fm reactions. This however, is presently impossible [20]. According to the macro-microscopic calculations one may expect a strong reduction in σ_{xn} values. At the same time according to microscopic calculations one could expect to observe reasonably high σ_{xn} values.

Overall, it is evident that the projectile-target combination primarily defines the fusion probability. As seen in Fig. 3(b), the fusion probabilities of the other three reactions leading to element 120 will be further reduced. One can estimate that the reaction ^{54}Cr+^{248}Cm will probably have ≈ 3.6 times smaller σ_{xn} values than the ^{50}Ti-induced reactions, which will require reaching a cross-section sensitivity below 20 fb. Consequently, the reactions with heavier projectiles (^{58}Fe, ^{64}Ni etc.,) will suffer from a further reduction of P_{CN}. Therefore, ^{50}Ti-induced reactions are the most promising for exploring the discoveries of elements beyond Og. However, a final justification of these predictions has to come from the observation of the elements 119 and 120.

For the synthesis of element 119 another potential reaction is ^{51}V+^{248}Cm, which leads to the same CN as the ^{50}Ti+^{249}Bk reaction. According to the discussions above, one could expect a roughly two times smaller P_{CN} for the ^{51}V+^{248}Cm reaction compared with ^{50}Ti+^{249}Bk for which presently reached cross-section sensitivity is 65 pb. This would require to perform an experiment for the former reaction at the cross-section sensitivity on the order of at least 30 fb at a beam energy corresponding to the maximum of either the 3n or the 4n channel.

V. SUMMARY AND CONCLUSION

A four-months long experiment with a high intensity ^{50}Ti beam bombarding ^{249}Bk/^{249}Cf targets was carried out successfully at the gas-filled recoil separator TASCA. In the data collected during this challenging experimental campaign, we searched for correlated α-decay chains from isotopes of the new elements 119 and 120. We did not observe any non-random α-decay chain terminating with a fission that could be attributed to the decay of superheavy nuclei with $Z = 119$ and 120. This resulted in "one event" cross-section sensitivities of 65 fb and 200 fb for the ^{50}Ti+^{249}Bk and ^{50}Ti+^{249}Cf reactions, respectively, at a mid-target beam energy of $E_{\rm lab} = 281.5$ MeV.

These cross-section sensitivity levels are not applicable if the isotopes of the element 119 and 120 would directly decay either by spontaneous fission and/or electron-capture delayed fission for which recent calculations show non-negligible probabilities [49, 50]. In the present work unambiguous identification of such direct fission decays, i.e., ER–SF from SHN was not possible. However, in the future one should consider the search for unknown spontaneous fission or electron-capture delayed fission branches of SHN, which would reduce the identification efficiency of SHN via α-decay chains.

The non-observation of isotopes of elements 119 and 120 was discussed within the context of the fusion-evaporation reaction mechanism. It is apparent that the fusion probability of ^{50}Ti and heavier projectiles with actinide targets is significantly reduced compared to ^{48}Ca-induced reactions. The present combinations, ^{50}Ti+^{249}Bk and ^{50}Ti+^{249}Cf, are still considered as the most promising reactions for the syntheses of the next two elements beyond Og. However, for the observation of evaporation residues from these reactions, experiments need to be carried out that reach much smaller cross-section levels, as compared with the ones presently obtained.

VI. ACKNOWLEDGEMENTS

We are grateful for GSI's Penning ion-source and UNILAC staff, and the Experimental Electronics department for their continuous support of the experiment. This work was financially supported in part by the German BMBF (05P12UMFNE), the Helmholtz association (VH-NG-723), the Helmholtz Institute Mainz, Swedish Research Council (Vetenskapsrådet, VR 2011-5253 and VR 2016-3969), the Australian Federal Government ARC grants (DP170102318, DP170102423 and DP200100601), the U.S. Department of Energy by LLNL (DE-AC52-07NA27344), Vanderbilt University Grant No. DE-FG05-88ER40407, the Laboratory Directed Research and Development Program at LLNL (11-ERD-011). This work was co-sponsored by the Office of Science, U.S. Department of Energy, and supported under U.S. DOE grant No. DE-AC05-00OR22725.

[1] Yu. Ts. Oganessian and V. K. Utyonkov, Rep. Prog. Phys. **78**, 036301 (2015).
[2] Special Issue on Superheavy Elements, Nucl. Phys. A **944** (2018).
[3] Yu. Ts. Oganessian, A. Sobiczewski, and G. M. Ter-Akopian, Phys. Scr. **92**, 023003 (2017).
[4] S. Giuliani *et al.*, Rev. Mod. Phys. **91**, 011001 (2019).
[5] S. Hofmann *et al.*, Eur. Phys. J. A **32**, 251 (2007).
[6] L. Stavsetra *et al.*, Phys. Rev. Lett. **103**, 132502 (2009).
[7] Ch. E. Düllmann *et al.*, Phys. Rev. Lett. **104**, 252701 (2010).
[8] P. A. Ellison *et al.*, Phys. Rev. Lett. **105**, 182701 (2010).
[9] J. M. Gates *et al.*, Phys. Rev. C **83**, 054618 (2011).
[10] S. Hofmann *et al.*, Eur. Phys. J. A **48**, 62 (2012).
[11] D. Rudolph *et al.*, Phys. Rev. Lett. **111**, 112502 (2013).
[12] J. Khuyagbaatar *et al.*, Phys. Rev. Lett. **112**, 172501 (2014).
[13] U. Forsberg *et al.*, Nucl. Phys. A **953**, 117 (2016).
[14] D. Kaji *et al.*, J. Phys. Soc. Japan **86**, 034201 (2017).
[15] J. M. Gates *et al.*, Phys. Rev. Lett. **121**, 222501 (2018).
[16] J. Khuyagbaatar *et al.*, Phys. Rev. C. **99**, 054306 (2019).
[17] M. G. Itkis *et al.*, Nucl. Phys. A **787**, 150 (2007).
[18] J. Khuyagbaatar, EPJ Web of Conferences **163**, 00030 (2017).
[19] J. Khuyagbaatar, EPJ Web of Conferences **163**, 00068 (2017).

[20] J. Roberto *et al.*, Nucl. Phys. A **944**, 99 (2015).
[21] S. Hofmann *et al.*, GSI Scientific Report 2007 , 131 (2008).
[22] Yu. Ts. Oganessian *et al.*, Phys. Rev. C **79**, 024603 (2009).
[23] S. Hofmann *et al.*, Eur. Phys. J. A **52**, 180 (2016).
[24] Ch. E. Düllmann *et al.*, to be published..
[25] H. M. Albers *et al.*, Phys. Lett. B **808**, 135626 (2020).
[26] J. Chen *et al.*, Phys. Rev. C **90**, 044302 (2014).
[27] Yu. Ts. Oganessian *et al.*, Phys. Rev. Lett. **109**, 162501 (2012).
[28] J. Runke *et al.*, J. Rad. Nucl. Chem. **299**, 1081 (2014).
[29] J. Khuyagbaatar *et al.*, GSI Scientific Report 2012 , 131 (2013).
[30] E. Jäger *et al.*, J. Rad. Nucl. Chem. **299**, 1073 (2014).
[31] J. F. Ziegler, Nucl. Inst. Meth. B **219**, 1027 (2004).
[32] G. Audi, A. Wapstra, and C. Thibault, Nucl. Phys. A **729**, 337 (2003).
[33] W. Myers and W. Swiatecki, Nucl. Phys. A **601**, 141 (1996).
[34] V. Zagrebaev and W. Greiner, Phys. Rev. C **78**, 034610 (2008).
[35] A. Semchenkov *et al.*, Nucl. Inst. Meth. B **266**, 4153 (2008).
[36] J. Khuyagbaatar *et al.*, Nucl. Inst. Meth. A **689**, 40 (2012).
[37] K. Gregorich, Nucl. Inst. Meth. A **711**, 47 (2013).
[38] J. Khuyagbaatar *et al.*, Phys. Rev. A **88**, 042703 (2013).
[39] A. Gorshkov, *A new focal plane detector for the gas-filled separator TASCA*, Ph.D. thesis, Technical University of Munich (2010).
[40] I. Wegrzecka *et al.*, Proc. SPIE. **8902** (2013), 10.1117/12.2031044.
[41] J. Khuyagbaatar *et al.*, Phys. Rev. Lett. **115**, 242502 (2015).
[42] N. Kurz *et al.*, GSI Scientific Report 2011 , 252 (2012).
[43] A. Di. Nitto *et al.*, Phys. Lett. B **784**, 199 (2018).
[44] J. Khuyagbaatar *et al.*, Nucl. Phys. A **994**, 121662 (2020).
[45] A. Såmark-Roth *et al.*, Phys. Rev. C **98**, 044307 (2018).
[46] J. Kallunkathariyil *et al.*, Phys. Rev. C **101**, 011301 (2020).
[47] J. N. P. Möller and K.-L. Kratz, At. Data and Nucl. Data Tables **66**, 131 (1997).
[48] R. Smolanczuk, Phys. Rev. C **56**, 812 (1997).
[49] J. Khuyagbaatar, Eur. Phys. J. A **55**, 134 (2019).
[50] J. Khuyagbaatar, Nucl. Phys. A **1002**, 121958 (2020).
[51] Yu. Ts. Oganessian *et al.*, Phys. Rev. C **87**, 034605 (2013).
[52] Yu. Ts. Oganessian *et al.*, Acta Phys. Slo. **49**, 65 (1999).
[53] J. Khuyagbaatar, to be published.
[54] J. Khuyagbaatar *et al.*, Eur. Phys. J. A **37**, 177 (2008).
[55] A. Lopez-Martens *et al.*, Phys. Lett. B **795**, 271 (2019).
[56] F. P. Hessberger, Eur. Phys. J. A **55**, 208 (2019).
[57] R. Bass, *Nuclear reactions with heavy ions* (Springer-Verlag, Berlin Heidelberg New York, 1980).
[58] T. Tanaka *et al.*, J. Phys. Soc. Japan **87**, 014201 (2018).
[59] T. Tanaka *et al.*, Phys. Rev. Lett. **124**, 052502 (2020).
[60] K. Hagino, N. Rowley, and A. T. Kruppa, Comp. Phys. Comm. **123**, 143 (1999).
[61] A. S. Umar, V. E. Oberacker, and C. Simenel, Phys. Rev. C **94**, 024605 (2016).
[62] R. Vandenbosch and J. R. Huizenga, *Nuclear Fission* (Academic Press, New York and London, 1973).
[63] J. Khuyagbaatar *et al.*, Phys. Rev. C **91**, 054608 (2015).
[64] J. Khuyagbaatar *et al.*, Phys. Rev. C **97**, 064618 (2018).
[65] K. Banerjee *et al.*, Phys. Rev. Lett. **122**, 232503 (2019).
[66] K. Nishio *et al.*, Phys. Rev. C **82**, 024611 (2010).
[67] R. Graeger *et al.*, Phys. Rev. C **81**, 061601 (2010).
[68] Z.-H. Liu and J.-D. Bao, Phys. Rev. C **84**, 031602 (2011).
[69] N. Wang, E.-G. Zhao, W. Scheid, and S.-G. Zhou, Phys. Rev. C **85**, 041601 (2012).
[70] L. Zhu, W.-J. Xie, and F.-S. Zhang, Phys. Rev. C **89**, 024615 (2014).
[71] N. Ghahramany and A. Ansari, Eur. Phys. J. A **52**, 287 (2016).
[72] G. Adamian, N. Antonenko, and H. Lenske, Nucl. Phys. A **970**, 22 (2018).
[73] P. Möller *et al.*, At. Data and Nucl. Data Tab. **59**, 185 (1995).
[74] A. Mamdouh, J. Pearson, M. Rayet, and F. Tondeur, Nucl. Phys. A **679**, 337 (2001).
[75] A. Staszczak, A. Baran, and W. Nazarewicz, Phys. Rev. C **87**, 024320 (2013).
[76] W. Swiatecki, Phys. Scr. **24**, 113 (1981).
[77] D. J. Hinde *et al.*, Phys. Rev. Lett. **74**, 1295 (1995).
[78] R. du Rietz *et al.*, Phys. Rev. C **88**, 054618 (2013).
[79] K. Nishio *et al.*, Phys. Rev. C **86**, 034608 (2012).
[80] A. Berriman *et al.*, Nature **413**, 144 (2001).
[81] D. Hinde and M. Dasgupta, Phys. Lett. B **622**, 23 (2005).
[82] G. Knyazheva *et al.*, Phys. Rev. C **75**, 064602 (2007).
[83] E. Kozulin *et al.*, Phys. Rev. C **94**, 054613 (2016).
[84] E. Kozulin *et al.*, Phys. Rev. C **99**, 014616 (2019).
[85] R. Yanez *et al.*, Phys. Rev. Lett. **112**, 152702 (2014).
[86] K. Hirose *et al.*, Phys. Rev. Lett. **119**, 222501 (2017).
[87] A. Baran, M. Kowal, P.-G. Reinhard, L. Robledo, A. Staszczak, and M. Warda, Nucl. Phys. A **944**, 442 (2015).
[88] P. Jachimowicz, M. Kowal, and J. Skalski, Phys. Rev. C **95**, 014303 (2017).
[89] P. Jachimowicz, M. Kowal, and J. Skalski, Phys. Rev. C **101**, 014311 (2020).
[90] R. Rodriguez-Guzman, Y. M. Humadi, and L. M. Robledo, Eur. Phys. J. A **56**, 43 (2020).